fire

MDPI

Article

Investigation on Flexural Behavior of Galvanized Cold-Formed Steel Beams Exposed to Fire with Different Stiffener Configurations

Varun Sabu Sam [1], Garry Wegara K Marak [1], Anand Nammalvar [1,*], Diana Andrushia [2], Beulah Gnana Ananthi Gurupatham [3] and Krishanu Roy [4,*]

[1] Department of Civil Engineering, Karunya Institute of Technology and Sciences, Coimbatore 641114, India; varunsabu21@karunya.edu.in (V.S.S.); garrywegaramarak@karunya.edu.in (G.W.K.M.)
[2] Department of Electronics and Communication Engineering, Karunya Institute of Technology and Sciences, Coimbatore 641114, India; diana@karunya.edu
[3] Division of Structural Engineering, College of Engineering Guindy Campus, Anna University, Chennai 600025, India; beulah28@annauniv.edu
[4] School of Engineering, The University of Waikato, Hamilton 3216, New Zealand
* Correspondence: nanand@karunya.edu (A.N.); kris.roy@waikato.ac.nz (K.R.)

Abstract: Cold-formed steel (CFS) sections, increasingly favored in the construction industry due to their numerous advantages over hot-rolled steel, have received limited attention in research concerning the flexural behavior of galvanized iron (GI)-based CFS at elevated temperatures. Understanding how these materials and structures behave under elevated temperatures is crucial for fire safety. The authors have performed experimental studies previously on GI-based CFS under elevated temperatures. In that study, CFS sections made of GI of grade E350 of 1.5 m long and 2 mm thickness were used. Built-up beam sections were tested under two-point loading after heating to 60 and 90 min durations and subsequently cooling them down using air and water. This study aims to uncover the influence of different stiffener configurations on the load carrying capacity of sections under elevated temperature parametrically. With the experimental study results from previous studies as a reference, authors used FEM analysis to comprehensively study the behavior of GI-based CFS sections under fire. Vertical, horizontal, and not providing a stiffener were the configurations selected to study the beams parametrically. Parametric analysis confirmed that different stiffener configurations did not alter the predominant failure mode, which remained distortional buckling across all specimens. Beams with vertical stiffeners demonstrated superior performance compared to those with horizontal stiffeners in parametric analysis. Lateral–torsional buckling was observed in the reference specimen, lacking stiffeners due to inadequate restraint at the supports.

Keywords: flexural behavior; cold-formed steel; fire; post-fire behavior; stiffeners; parametric study

Citation: Sam, V.S.; Marak, G.W.K.; Nammalvar, A.; Andrushia, D.; Gurupatham, B.G.A.; Roy, K. Investigation on Flexural Behavior of Galvanized Cold-Formed Steel Beams Exposed to Fire with Different Stiffener Configurations. *Fire* **2024**, *7*, 318. https://doi.org/10.3390/fire7090318

Academic Editor: Tiago Miguel Ferreira

Received: 14 July 2024
Revised: 28 August 2024
Accepted: 11 September 2024
Published: 13 September 2024

1. Introduction

Cold-formed steel (CFS) is gaining popularity in the construction industry due to its high strength-to-weight ratio, ductility, availability, and ease of construction. Unlike hot-rolled steel, CFS is formed without the application of heat during manufacturing, using processes such as rolling, bending, pressing, and stamping to achieve desired shapes and sizes. It retains steel's inherent properties such as ductility, strength, and durability well and is available in various grades and thicknesses to meet specific requirements. Its lightweight nature makes it easier to handle and transport, leading to cost savings in large construction projects. The high strength-to-weight ratio of CFS provides robust structural support while keeping overall weights low, which is beneficial, especially in seismic zones where it reduces foundation loads significantly. Consistent quality and dimensions across sections make CFS ideal for applications requiring precise fit and performance, thereby reducing labor costs and installation time.

Despite these advantages, CFS has drawbacks, such as lower fire resistance compared to conventional steel. However, this can be mitigated with fireproof coatings and protective methods. To promote greater use of CFS, it is crucial to study its behavior after exposure to fire and develop strategies to minimize fire damage.

Stiffeners are structural elements used to reinforce or strengthen other members, preventing them from buckling or deforming under load. They are often employed in thin-walled structures, such as plates, beams, and shells, where the primary member may be susceptible to local buckling or excessive deflection. Stiffeners increase the load-carrying capacity, stability, and stiffness of the structure. They help in distributing loads more evenly across the structural member, reducing stress concentrations and improving the overall performance. They also effectively increase the buckling resistance of thin-walled sections, allowing them to carry higher loads without failure. They are commonly used in beams and girders, especially at locations of high shear forces, such as near supports and load application points. There are mainly vertical, horizontal, and cross stiffeners provided as per design requirements. Several design codes like AISI and Euro code 3 [1,2] provide guidelines on the design of stiffeners in steel structures, including minimum thickness, spacing, and connection details.

Several studies have investigated various aspects of CFS behavior, such as structural performance under bending, torsion, bolted connections, and the influence of design parameters like hole size and section slenderness [3–11]. These studies have led to advancements in design equations and guidelines for CFS applications [12–20].

The evaluation of the Direct Strength Method (DSM) for single-span lipped channel beams under high temperatures, as conducted by [21], revealed that the existing DSM distortional strength curve is insufficient for accurately predicting beam failure moments in such conditions. This underscores the need for more precise predictive models tailored to high-temperature scenarios.

Experimental and numerical studies on CFS built-up sections, particularly focusing on back-to-back sigma sections, were undertaken by [22]. Their research, which validated various section lengths and proposed new guidelines, highlights the importance of a comprehensive analysis of different configurations and lengths when assessing structural performance under elevated temperatures.

The behavior of CFS galvanized iron (GI) beams during fire scenarios was also examined by [22], concluding that the choice to use CFS beams with or without web stiffeners should be based on the section shape and the internal forces acting on the beams during a fire. This finding aligns with our investigation into the effects of different beam configurations on performance at elevated temperatures.

The collapse behavior of a single-story CFS building under severe fire conditions was explored by [23], where a finite element model was developed to simulate the behavior of CFS cantilever wall systems in such scenarios. The flexural behavior of CFS square and rectangular sections subjected to heat treatment was investigated by Pannuzzo and Chan [24] through numerical methods, leading to the proposal of new design limits based on various codes. Their work, along with that in [25] wherein the authors assessed the flexural strength of CFS oval hollow section beams and confirmed the validity of the DSM and continuous strength methods, supports the thoroughness of this study's methodology and its significance in improving design approaches for CFS beams in high-temperature conditions.

The key innovation of this article lies in its investigation of the flexural behavior of CFS beams with various stiffener configurations under fire conditions, including different heating and cooling regimes. Previous research, such as the study referenced [DOI: 10.3390/buildings14082456], has primarily focused on geometric variations and their effects on flexural strength and failure modes, but it has not addressed the impact of stiffeners in fire scenarios. This paper explores how different types of stiffeners—vertical, horizontal, and no stiffener—affect the stability and flexural behavior of CFS beams during fires. Stiffeners significantly enhance the load capacity and stability of CFS elements by preventing local buckling. The study fills a research gap by evaluating the influence of stiffeners on the

load–deflection characteristics (stiffness, ductility, and energy absorption capacity) of CFS beams under fire exposure and varying cooling methods. The paper also examines how different heating and cooling regimes, as per ISO standards, affect the flexural behavior and failure modes of CFS beams with various stiffener configurations.

In addition, by comparing air-cooling and water-cooling methods, this study sheds light on the effects of different cooling regimes on the structural integrity of CFS beams after heating. This aspect is crucial for developing effective fire safety protocols. The combination of experimental findings with Finite Element Modeling (FEM) using ABAQUS and Direct Strength Method (DSM) results ensures robust validation, thereby enhancing the reliability of the findings.

In fire scenarios, maintaining the structural integrity of building components is paramount. By examining how CFS beams behave under elevated temperatures, this research contributes to the development of safer construction practices and fire-resistant designs. The findings can inform the design and optimization of CFS beams, leading to more efficient use of materials and improved performance in fire scenarios. This has direct implications for the construction industry, where CFS is increasingly used in residential and commercial buildings.

Moreover, the results of this study can provide valuable data for updating building codes and standards, ensuring that they adequately address the fire performance of CFS structures.

The primary problem addressed by this study is the lack of a comprehensive understanding of the flexural behavior of galvanized iron (GI)-based CFS beams under elevated temperatures, particularly in relation to different stiffener configurations, heating durations, and cooling methods. While previous research has focused on specific aspects of CFS performance, there is a notable gap in the literature concerning the combined effects of these variables.

This study's aims are as follows:

- Analyze how various stiffener configurations (vertical, horizontal, and no stiffeners) influence the buckling behavior and ultimate load capacity of CFS beams under thermal loads.
- Evaluate the impact of different heating durations on the mechanical properties and failure modes of CFS beams.
- Determine the effects of air cooling versus water cooling on the post-heating performance of CFS beams.

By addressing these gaps, the study provides a more holistic understanding of the factors affecting the structural integrity and performance of CFS beams in fire scenarios, contributing valuable insights for improved fire safety and design practices.

This paper is organized into several sections to provide a comprehensive understanding of the study on the flexural behavior of CFS beams made of GI under elevated temperatures. The sections in this study are the introduction, experimental data, numerical and parametric study, and DSM method. This paper also includes a signature curve, obtained using the software CUFSM (V5.04) [26].

2. Experimental Data

2.1. Configuration

GI-based CFS sections were chosen with grade 350, with a length of 1.5 m. These C-sections were connected back-to-back using self-tapping screws, as illustrated in Figure 1. The screws used for the web connections had a diameter of 6 mm. Pinned and roller supports were implemented at both ends to provide stability. After the sheet was shaped into the desired form through the cold roll forming process, the sections were assembled into back-to-back built-up configurations. Geometric imperfections that arise during this process can have a considerable impact on the buckling behavior and other failure modes of the CFS sections. These initial imperfections were meticulously measured for all test specimens [27].

Figure 1. Beam sections connected using self-tapping screws [27].

2.2. Heating and Cooling Regime

Multiple thermocouples were attached at various points along the length and cross-section of the beams to track temperature variations in real-time and adjust the heating process as needed. While slight temperature variations were observed due to factors such as thermocouple placement and the material's heat conduction properties, these variations were within an acceptable range and did not significantly deviate from the target temperature. Galvanized iron, being a relatively uniform heat conductor, was suitable for applications requiring consistent heat transfer. Air-cooled sections were removed from the furnace and left at room temperature (30–35 °C) until they returned to ambient conditions. For water-cooled sections, water was poured on the surface immediately after heating. Laboratory experiments inherently come with various sources of uncertainty and potential errors. Non-uniform temperature distribution during the heating process can significantly impact the experimental results. Efforts were made to maintain a consistent temperature across the length of the beam using controlled heating environments. Despite efforts to ensure uniform heating, slight temperature variations occurred due to factors like thermocouple positioning and material properties [27]. Figure 2 shows comparison of ISO fire curve and section surface temperature and rate of cooling using air and water.

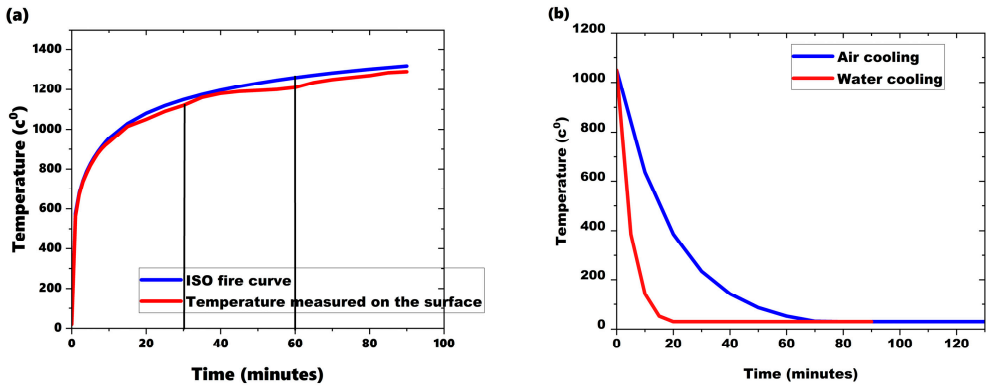

Figure 2. (**a**) Comparison of ISO fire curve and sections surface temperature, (**b**) rate of cooling using air and water.

2.3. Flexure Test

After heating and cooling, the beams were tested under two-point loading using a universal testing machine (UTM) to simulate their flexural behavior. Deflection meters were placed below the bottom flange at midpoint and loading points, while an LVDT measured displacement at the web. The load was applied at a constant displacement rate of 2 mm/min until the beams reached their ultimate load capacity and subsequent failure. Despite efforts to ensure uniform heating, slight temperature variations could affect material properties and failure modes. Instruments were calibrated before testing to minimize inaccuracies, though minor errors due to drift or positioning might still occur [27].

2.4. FEM Analysis

In this study, parametric analysis was conducted using FEM to investigate the flexural behavior of GI CFS beams with varying stiffener configurations, including vertical stiffeners, horizontal stiffeners, and no stiffeners. This analysis aimed to evaluate how different stiffener arrangements impact the beams' performance under loading in fire.

3. Numerical and Parametric Study

Parametric analysis and Finite Element Modeling (FEM) of all back-to-back GI-based CFS beams were conducted using ABAQUS software (2019_09_13-23.19.31) [28]. The dimensions, support conditions, and loading conditions used in the experimental tests were replicated in the ABAQUS models to simulate the same behaviors observed in experiments and to validate the results. The governing equations in ABAQUS are based on the principles of continuum mechanics. The software solves the equilibrium equations, which are expressed in terms of stresses, strains, and displacements.

Figure 3 illustrates the FEM models of the beam sections with vertical stiffeners. Initially, the beam sections were drawn in two dimensions and subsequently converted into three-dimensional models. These models were constructed to match the exact dimensions of the beams used in experimental studies.

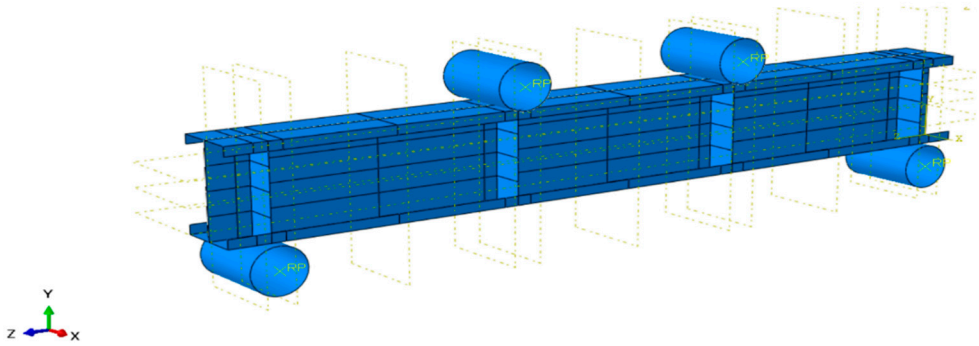

Figure 3. FEM model of beam with vertical stiffener.

By employing ABAQUS, the aim was to analyze the structural response under varying conditions, including high temperatures and various cooling methods, thereby providing a comprehensive understanding of the behavior of CFS beams made of GI in practical applications.

3.1. Material Properties

Material properties for the analysis of CFS beam sections made of GI were determined from coupon test results. The properties include Young's modulus, ultimate stress, yield stress, and Poisson's ratio, which were used as inputs for the modeling process. These properties were obtained from specimens fabricated from the same batch of material, as reported in [29], and are detailed in Table 1. Changes in ultimate load, yield strength, elastic modulus, and stress–strain values have been carefully studied and utilized for this study.

Engineering stress–strain values were measured and subsequently converted into true stress and strain using Equations (1) and (2). This conversion ensures an accurate representation of the material behavior under varying load conditions in the ABAQUS simulations.

$$\sigma_{true} = \sigma(1 + \epsilon) \tag{1}$$

$$\varepsilon_{true(pl)} = ln(1 + \varepsilon) - \frac{\sigma_{true}}{E} \tag{2}$$

where σ_{true} and $\varepsilon_{true(pl)}$ is representing true stress and true log plastic strain. σ and ε are engineering stress and strain.

Table 1. Material properties from coupon test.

Duration of Heating	Yield Strength Air Cooled (MPa)	Yield Strength Water Cooled (MPa)	Ultimate Strength Air Cooled (MPa)	Ultimate Strength Water Cooled (MPa)	Elastic Modulus Air Cooled (GPa)	Elastic Modulus Water Cooled (GPa)
Reference	349.62	349.62	451.13	451.13	205	205
30 min	289.42	251.32	397.56	394.54	150	148
60 min	201.07	194.91	264.76	255.76	130	123
90 min	170	156.4	213.34	197.89	94	93

3.2. Element Type and Meshing

All GI-based CFS beam sections were modeled using S4R elements, which are commonly used for modeling built-up sections, according to the literature. The mesh size plays a critical role in FE analysis, impacting both computation time and result accuracy [13]. An initial mesh was generated using a coarse mesh size, ensuring that the overall geometry and key features of the beams were captured. Quadratic elements were used for better accuracy in capturing stress distributions and deformations. The mesh was gradually refined by decreasing the element size, and the FEM simulations were rerun for each refined mesh. The ultimate load and deformation results were recorded for each mesh configuration. The results from successive mesh refinements were compared to establish a convergence criterion. When the variation in results (e.g., ultimate load and maximum deflection) between successive mesh refinements became negligible (typically less than 2%), the mesh was considered sufficiently fine. Based on the convergence analysis, a final mesh size was selected that balanced computational efficiency with result accuracy. This mesh was used for the detailed FEM simulations. Based on this and previous studies, a mesh size of 5 × 5 mm was selected for this study. Figure 4 illustrates the meshed CFS beam section without stiffeners. Tie constraints were utilized to connect both channels in place of self-tapping screws.

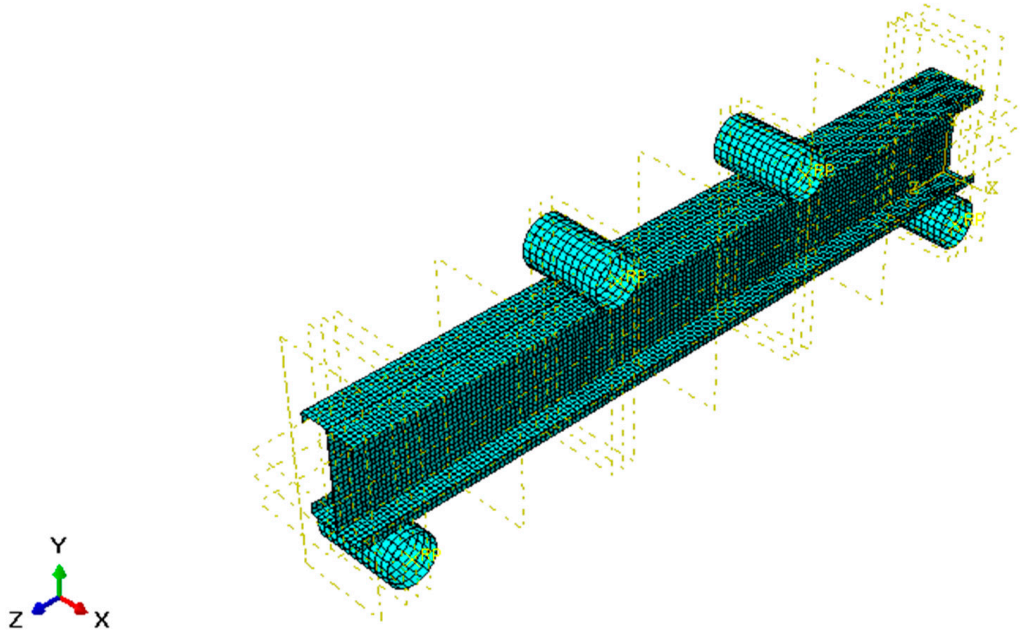

Figure 4. FEM model—meshing in beam section.

3.3. Loading and Boundary Conditions

Loading and boundary conditions were applied using two reference points located at the center of the loading plates and two additional points at the support regions. Degrees of freedom for translation and rotation were defined for these nodes after meshing. Initially, a linear bifurcation analysis was conducted, followed by a nonlinear analysis using the Modified Riks technique [12]. Eigenvalue analysis was performed to assess geometric imperfections in the FE models, and critical buckling modes were identified through linear bifurcation analysis. Table 2 lists the specimen IDs and their corresponding abbreviations used to identify each beam specimen.

Table 2. Specimen IDs.

Specimen ID	Definition of Section Type
	Experimental models (with vertical stiffener)
EREF	Unheated beam section
E60-AC	Beam heated for 60 min, cooled using air
E60-WC	Beam heated for 60 min, cooled using water
E90-AC	Beam heated for 90 min, cooled using air
E90-WC	Beam heated for 90 min, cooled using water
	FEM and Parametric models
VREF	Unheated beam section with vertical stiffeners
V60-AC	Beam with vertical stiffeners and heated for 60 min, cooled using air
V60-WC	Beam section with vertical stiffeners and heated for 60 min, cooled using water
V90-AC	Beam section with vertical stiffeners and heated for 90 min, cooled using air
V90-WC	Beam section with vertical stiffeners and heated for 90 min, cooled using water
HREF	Unheated beam section with horizontal stiffeners
H60-AC	Beam section with horizontal stiffeners and heated for 60 min, cooled using air
H60-WC	Beam section with horizontal stiffeners and heated for 60 min, cooled using water
H90-AC	Beam section with horizontal stiffeners and heated for 90 min, cooled using air
H90-WC	Beam section with horizontal stiffeners and heated for 90 min, cooled using water
NREF	Unheated beam section with no stiffeners
N60-AC	Beam section with no stiffeners and heated for 60 min, cooled using air
N60-WC	Beam section with no stiffeners and heated for 60 min, cooled using water
N90-AC	Beam section with no stiffeners and heated for 90 min, cooled using air
N90-WC	Beam section with no stiffeners and heated for 90 min, cooled using water

3.4. Validation

Experimental values are taken from the authors' other work [27] and compared with the results of this parametric study. Figure 5 compares the load-carrying capacities of sections with vertical stiffeners obtained from experiments and FEM simulations at various temperatures. The results from the FE analysis were found to align well with experimental results, showing good agreement with differences of less than 10.2% for reference specimens and less than 5.6% for all other sections. The failure modes predicted by the FEM, including buckling and yielding, were compared with the observed experimental failure modes. The FEM accurately predicted the location and type of failures, further validating the model.

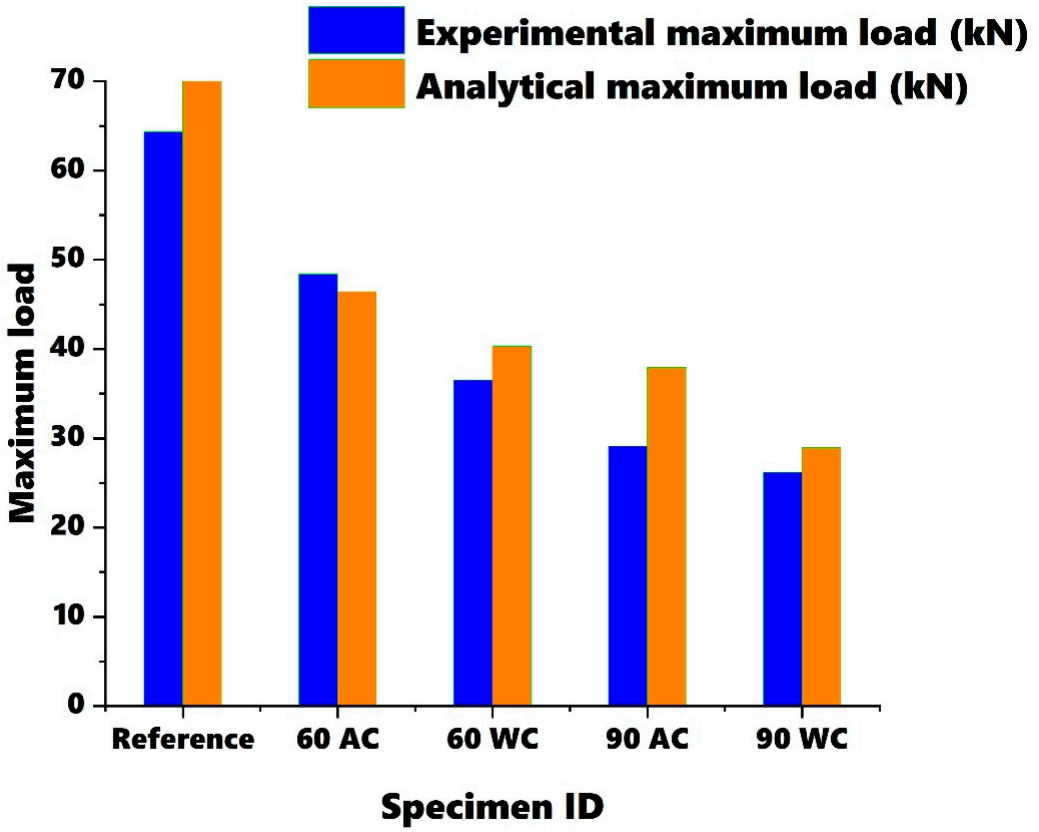

Figure 5. Validation of ultimate load between experimental and analytical model of the beam specimen with vertical stiffeners.

3.5. Failure Modes

Figures 6–8 illustrate that the type of stiffener did not significantly change the observed failure modes and patterns in beam specimens. For specimens with vertical and horizontal stiffeners, distortional buckling was the predominant failure mode. This shows that stiffeners effectively prevented lateral–torsional buckling, which is more likely to occur in members without stiffeners. The stiffeners provided additional lateral and torsional restraint, limiting the beam's tendency to twist and buckle under load. Both vertical and horizontal stiffeners led to similar failure modes, implying that the orientation of the stiffeners did not significantly alter the structural behavior under the conditions analyzed. Under heated conditions, the dominance of distortional buckling suggests that temperature increases reduced the material's yield strength and stiffness, making the sections more susceptible to buckling. The reduced stiffness and altered material properties likely made the beams more vulnerable to local instability, overriding the stiffeners' ability to fully stabilize the section. The impact of different cooling methods (air and water) on the observed failure modes could be critical. Rapid cooling (water) can induce thermal gradients and residual stresses, potentially exacerbating distortional buckling. On the other hand, slow cooling (air) might allow the material to relieve stresses more gradually, possibly reducing the severity of buckling.

However, beams without stiffeners exhibited both distortional buckling and lateral–torsional buckling (LTB) under ambient conditions. Under heated conditions, distortional buckling was the primary mode observed. Figure 8 details the failure modes observed in beam sections without stiffeners subjected to various durations of heating and cooling. Table 3 summarizes the failure modes identified in all FEM models analyzed, while Figure 9 graphically represents the failure modes for beams without stiffeners. Beams with vertical and horizontal stiffeners consistently exhibit distortional buckling during various heating

and cooling durations. In contrast, unstiffened sections fail through both distortional and lateral–torsional buckling, with lateral–torsional buckling typically occurring first.

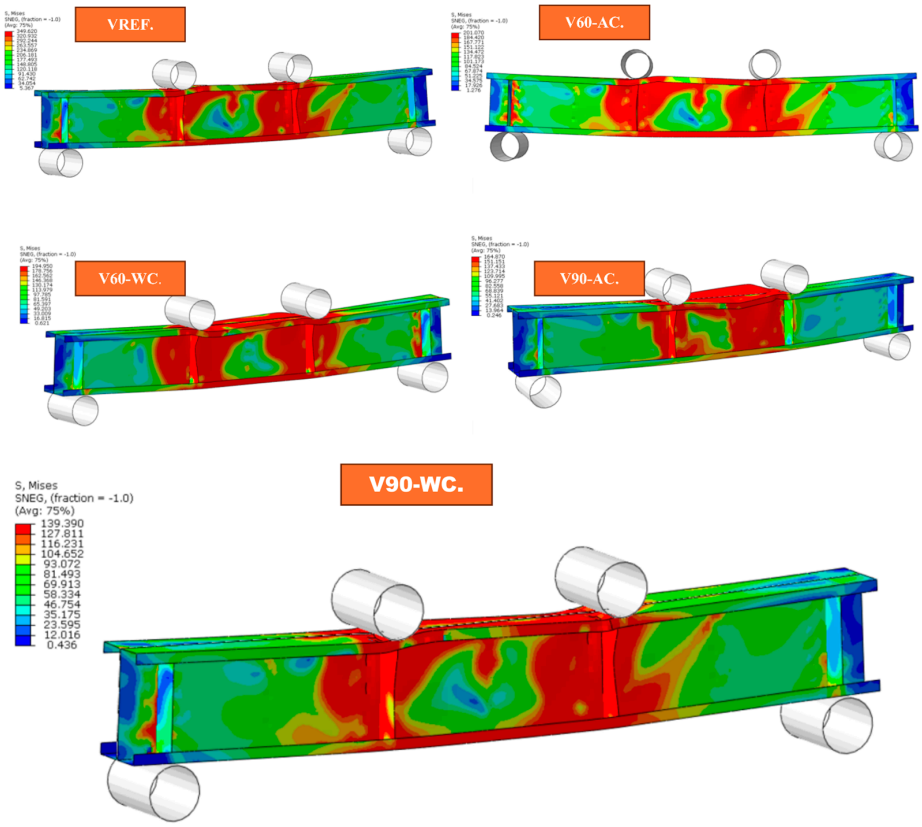

Figure 6. FEM failure modes of sections with vertical stiffener.

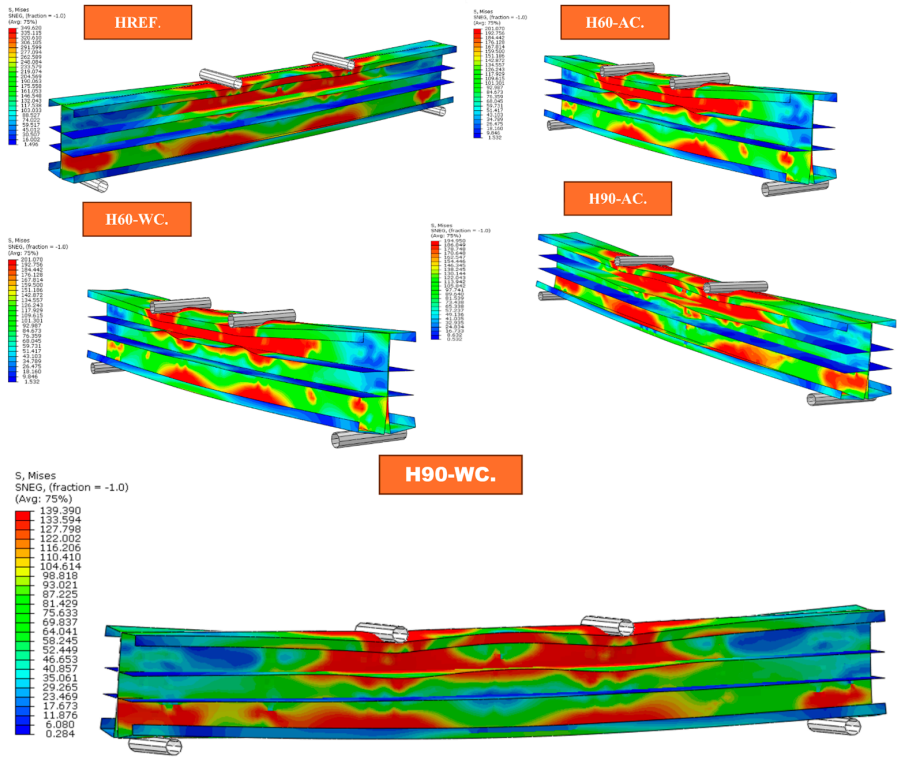

Figure 7. FEM failure modes of sections with horizontal stiffener.

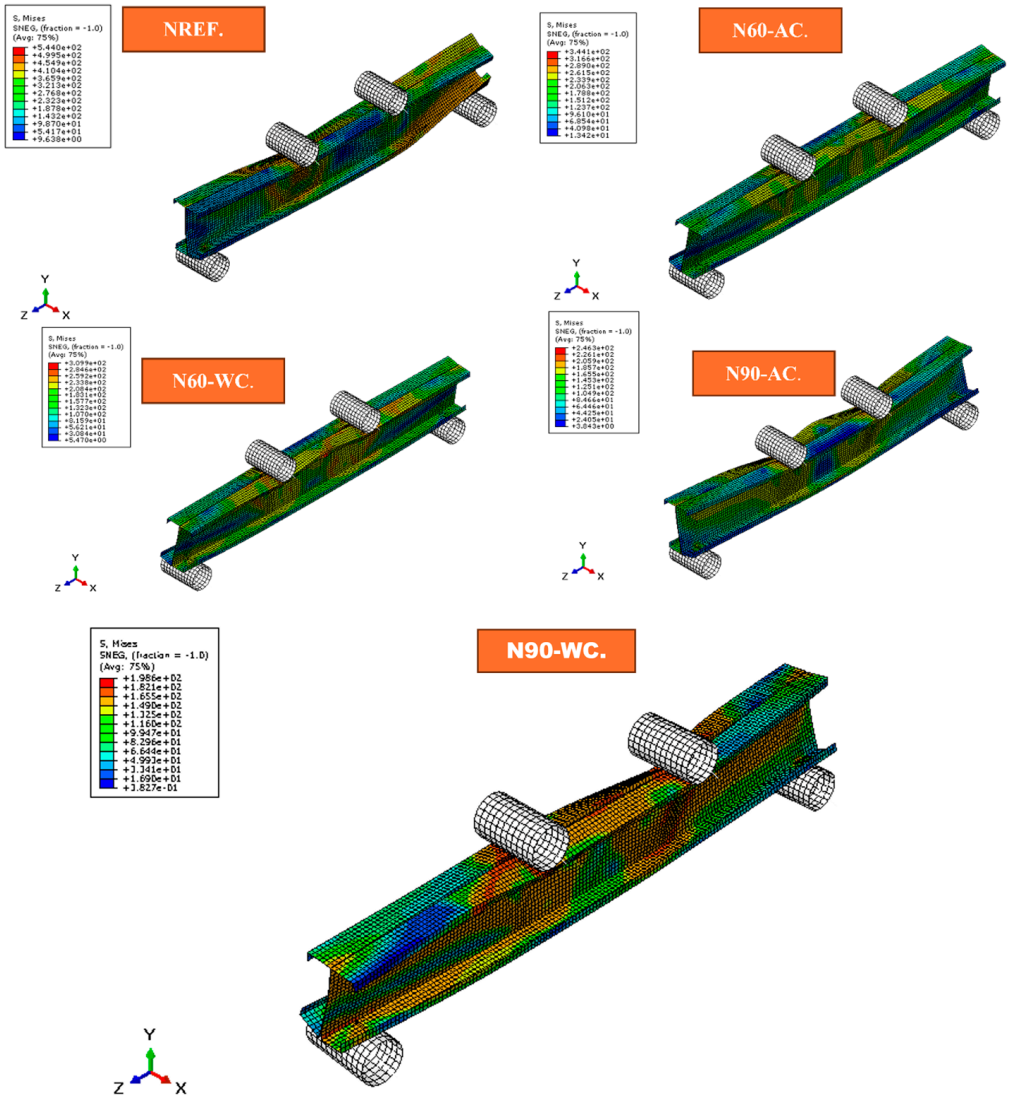

Figure 8. FEM failure modes of sections with no stiffener.

Table 3. Failure modes for all specimens.

Specimen ID	Failure Mode
Beams with no stiffener	
NREF	Lateral–torsional buckling and distortional buckling
N60-AC, N60-WC, N90-AC, N90-WC	Distortional buckling
Beams with vertical stiffener	
VREF, V60-AC, V60-WC, V90-AC, V90-WC	Distortional buckling
Beams with horizontal stiffener	
HREF, H60-AC, H60-WC, H90-AC, H90-WC	Distortional buckling

3.5.1. Comparison between Experimental and Analytical Load

The ultimate loads obtained experimentally [27] for sections with vertical stiffeners were compared with those for sections with horizontal stiffeners and no stiffeners through parametric analysis. Buckling behavior, failure modes, and failure mechanisms do not change depending on different heating and cooling conditions. But it changes depending on the stiffener provided. Figures 10 and 11 show the comparison of load-carrying capacities

between sections with vertical stiffeners, horizontal stiffeners, and no stiffeners. It was observed that sections with vertical stiffeners exhibited higher ultimate loads compared to those with horizontal stiffeners and no stiffeners. For instance, in the reference specimens, beams with vertical stiffeners showed load differences of 30.41% and 47.15% compared to beams with horizontal stiffeners and no stiffeners, respectively. Similarly, for beams heated for 60 min and cooled using water, differences of 26.43% and 43.01% were noted for beams with vertical stiffeners compared to those with horizontal stiffeners and no stiffeners, respectively. Figures 12–14 depict load–deflection values obtained for sections with different stiffeners analyzed through FEM. Vertical stiffeners provided significant improvement in the load-carrying capacity and stiffness of the beams. They effectively delayed local buckling and distributed the stresses more uniformly across the beam cross-section. The experimental results showed that beams with vertical stiffeners exhibited higher ultimate loads and reduced deflections compared to beams without stiffeners. Horizontal stiffeners also enhanced the beam performance but to a lesser extent compared to vertical stiffeners. They provided additional support to the web of the beam, reducing the likelihood of local buckling. However, the improvement in ultimate load and stiffness was not as pronounced as with vertical stiffeners. The experimental results indicated moderate increases in ultimate load and stiffness for beams with horizontal stiffeners. Beams without stiffeners demonstrated the lowest performance metrics. They were more prone to local buckling and exhibited lower ultimate loads and higher deflections under the same loading conditions. The absence of stiffeners resulted in a less uniform stress distribution and earlier onset of failure modes.

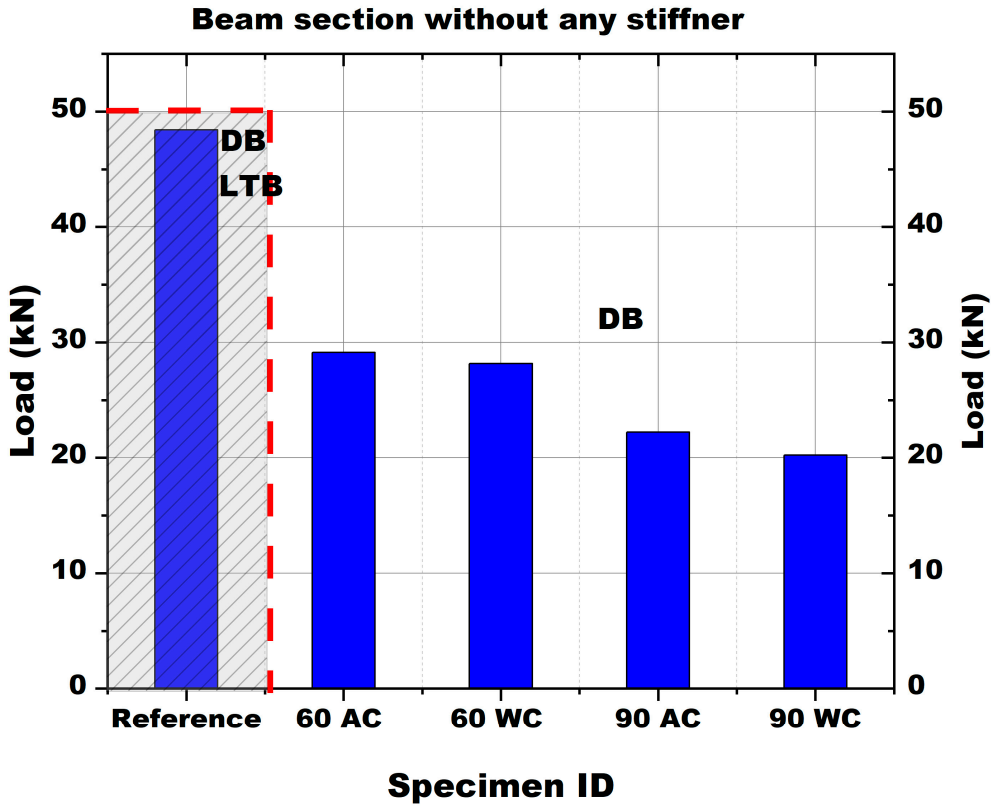

Figure 9. Failure modes noted for beam sections without any stiffener.

3.5.2. Energy Absorption Capacity

Energy absorption capacity (EAC) is a critical metric for assessing the performance of structural elements under dynamic or extreme conditions, such as fires or seismic events. It measures a material or structure's ability to absorb and dissipate energy without catastrophic failure. This property is especially important for CFS beams exposed to high temperatures.

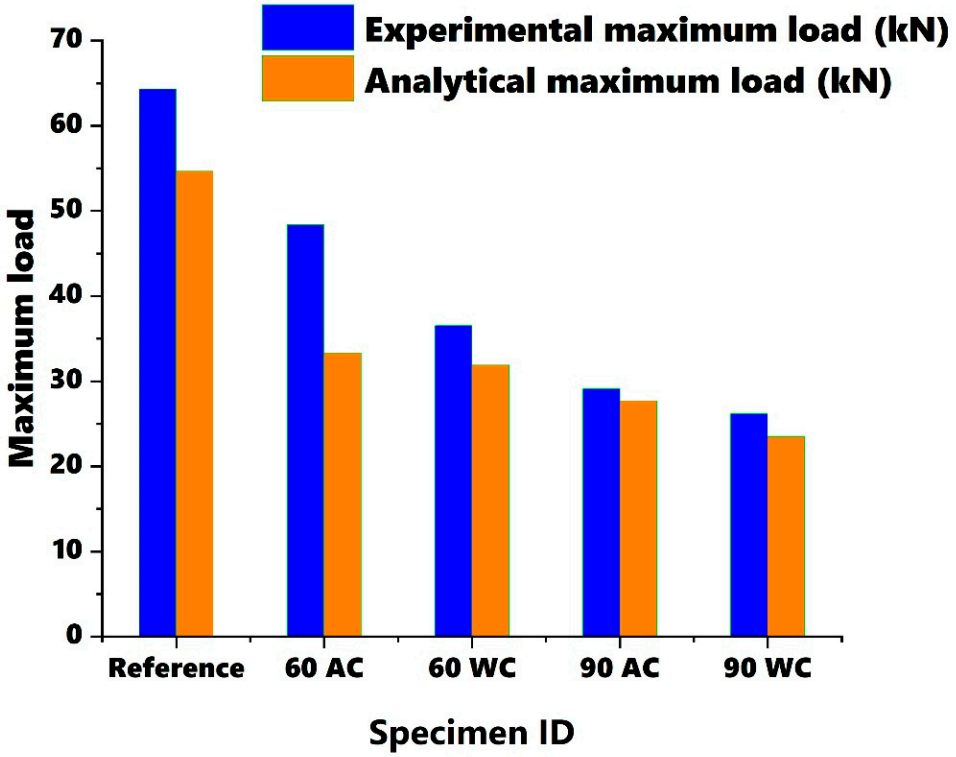

Figure 10. Comparison of ultimate load between experimental and analytical model of the beam specimen with horizontal stiffeners.

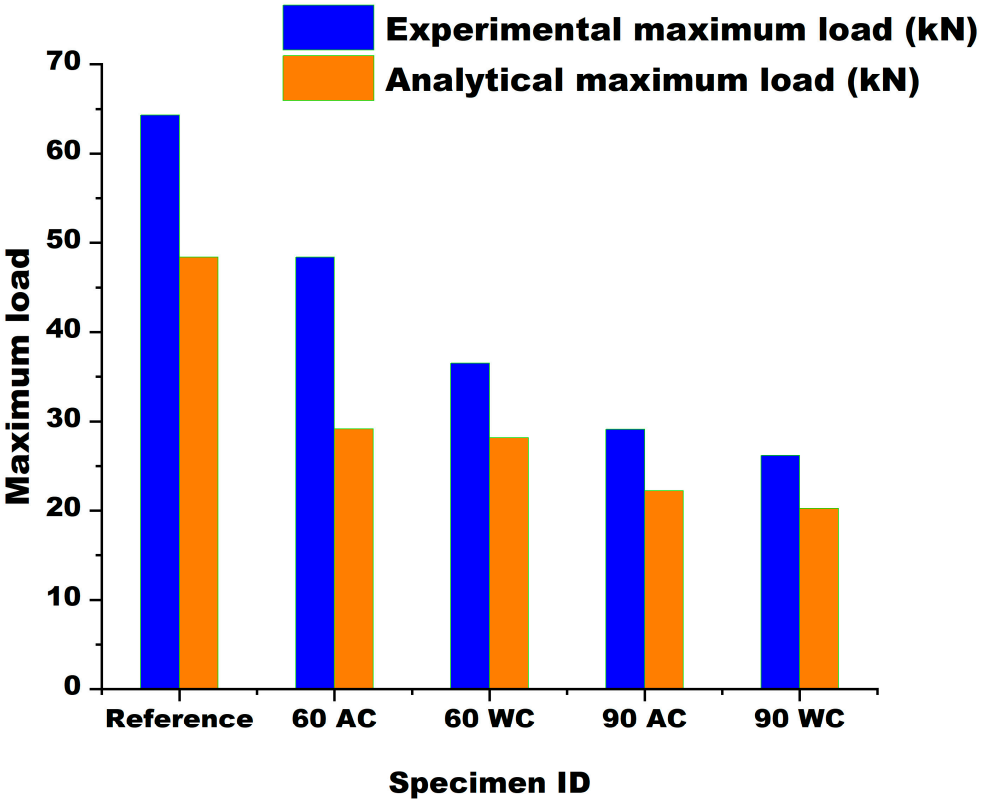

Figure 11. Comparison of ultimate load between experimental and analytical model of the beam specimen with no stiffeners.

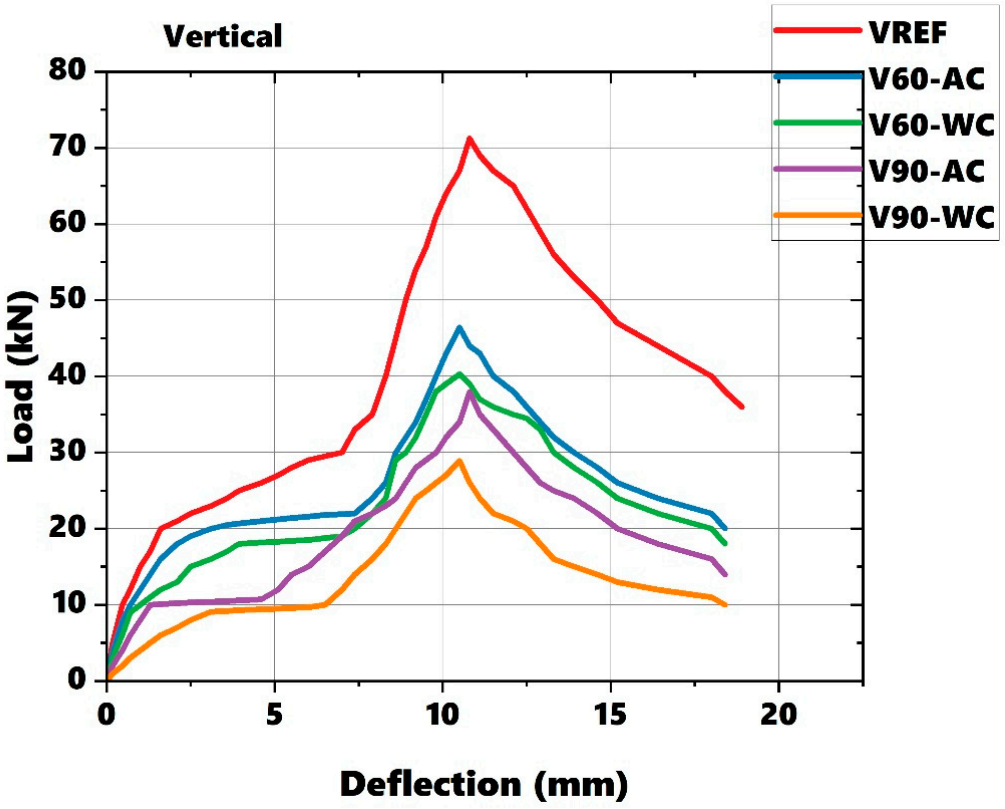

Figure 12. Load–deflection curve obtained for sections with vertical stiffener.

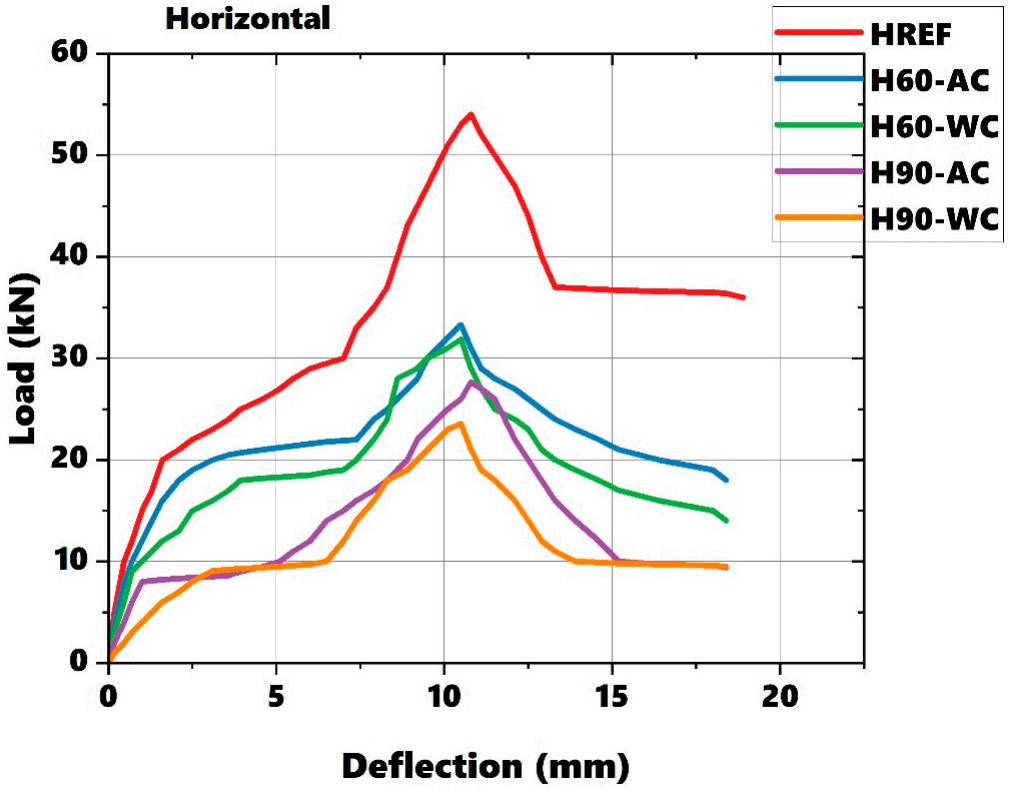

Figure 13. Load–deflection curve obtained for sections with horizontal stiffener.

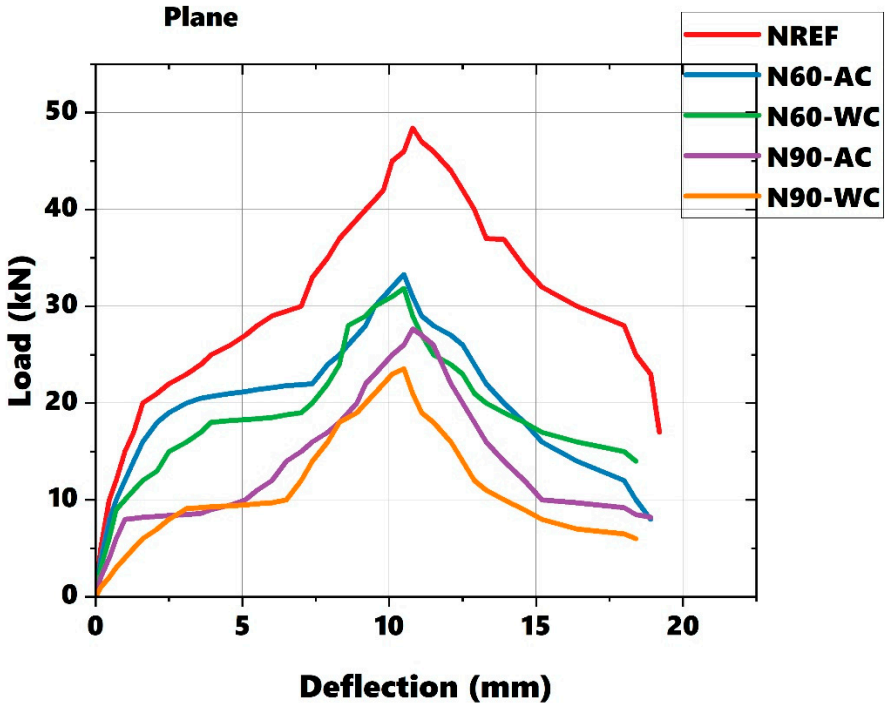

Figure 14. Load–deflection curve obtained for sections with no stiffener.

Figures 15 and 16 show the EAC values for sections with different stiffeners subjected to various heating and cooling durations. The data indicate that EAC decreases as heating duration increases. Specifically, for sections with horizontal stiffeners, the EAC of H60-AC is about 32.4% lower than HREF, showing significant degradation in energy absorption due to heating. The EAC of H90-AC is 59.6% lower than H60-AC, highlighting a substantial decline with further heating. A similar trend is observed in sections without stiffeners, with the EAC of N90-AC being 59.6% lower than N60-AC, demonstrating the impact of temperature on the reduction in flexural capacity.

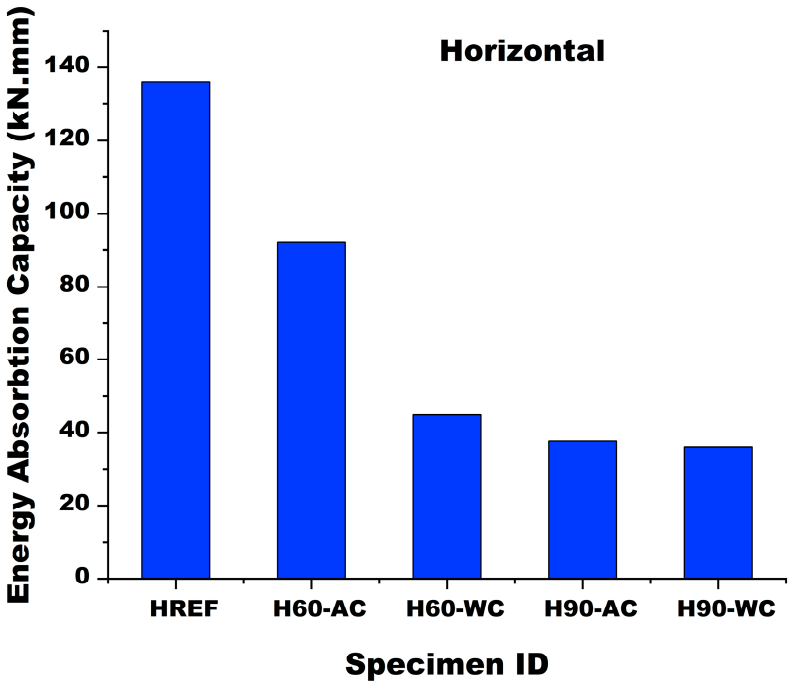

Figure 15. EAC for sections with horizontal stiffener.

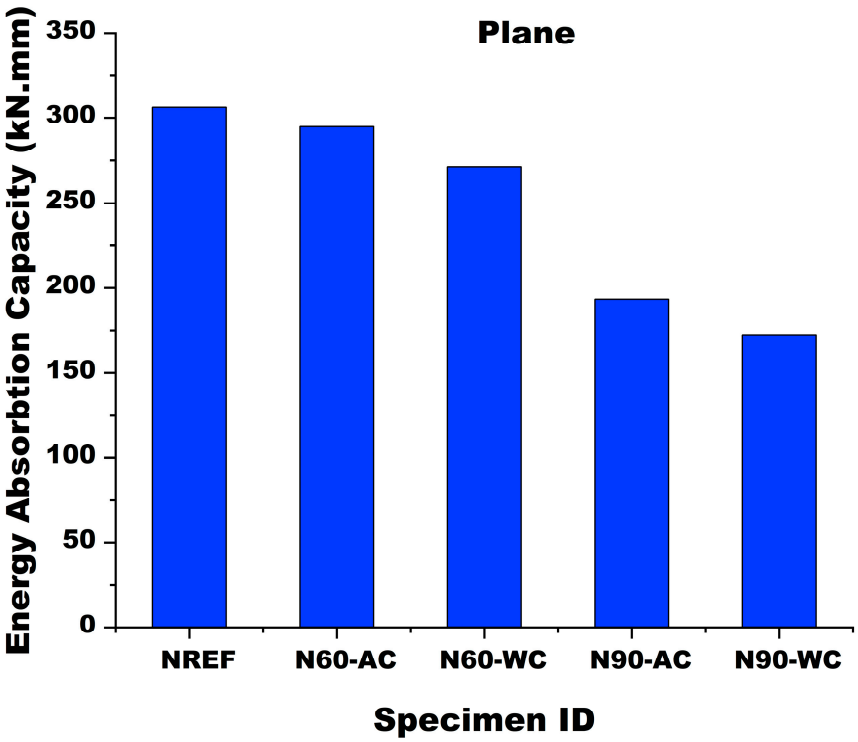

Figure 16. EAC for sections with no stiffener.

3.6. Stiffness

Figures 17 and 18 present the stiffness values for sections with horizontal stiffeners and sections without stiffeners under various heating and cooling durations. Stiffness is a critical property that reflects a material's or structure's resistance to deformation under load. Stiffness is calculated using the ultimate load with its corresponding deflection.

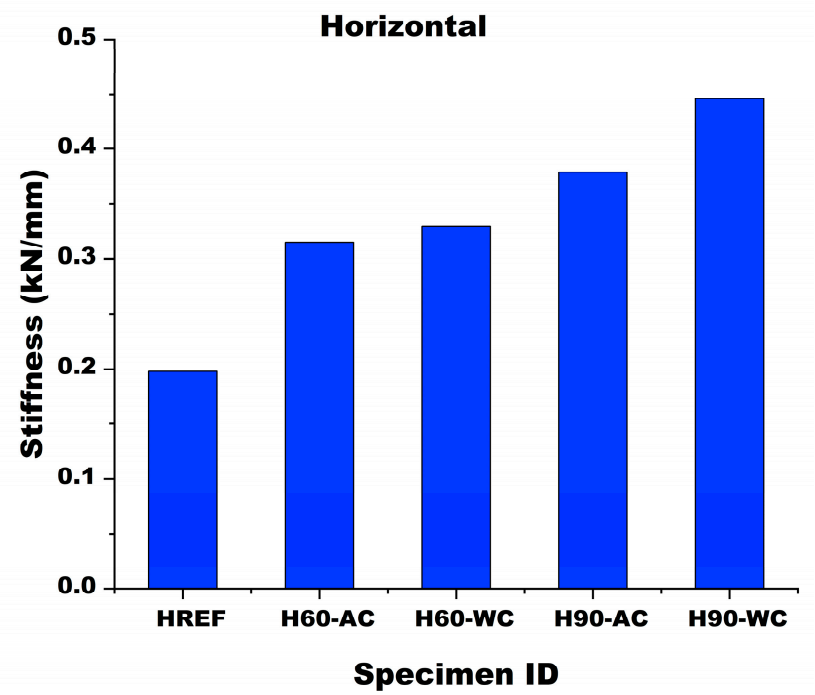

Figure 17. Stiffness for sections with horizontal stiffener.

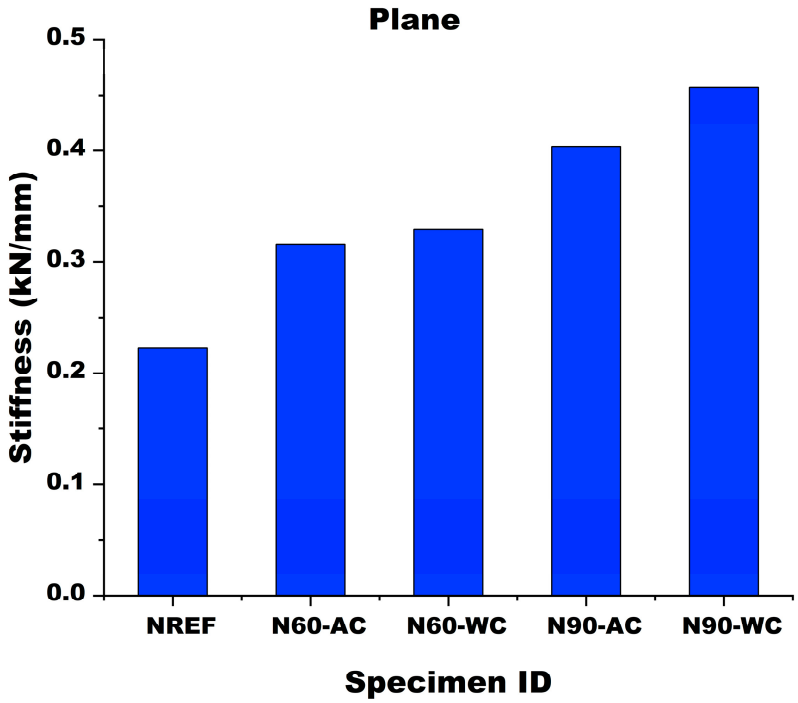

Figure 18. Stiffness for sections with no stiffener.

The figures show that stiffness generally increases with longer heating durations. For instance, the stiffness of H60-AC is approximately 59.1% higher than HREF, indicating a significant increase due to 60 min of heating with air cooling compared to an unheated specimen. Similarly, the stiffness of H90-WC is 35.6% higher than H60-WC, reflecting a notable increase with extended heating duration.

3.7. Ductility Factor

The ductility factor measures a material's ability to undergo significant plastic deformation before failure. It is defined as the ratio of energy absorbed during plastic deformation to that absorbed during elastic deformation. Ductility is evaluated from load–deflection diagrams by dividing the ultimate displacement by the yield displacement. Figures 19 and 20 depict ductility factor calculated for sections with different stiffeners subjected to various heating and cooling durations.

Water cooling results in a lower ductility factor compared to air cooling for the same heating duration. For example, after 60 min of heating, the ductility factor decreases by about 42.6% with water cooling compared to the reference specimen. Additionally, increased heating duration leads to a reduced ductility factor; for instance, the ductility factor decreases by about 11.7% with an additional 30 min of heating under air cooling and by 21.7% with water cooling.

3.8. Relationship

Figures 21–23 present the relationship between yield strength and ultimate moment values for beam sections with vertical, horizontal, and no stiffeners. The coefficient of determination (R2) values were calculated and found to be nearly equal to 1 for all sections. As the heating duration increased, both yield strength and moment of resistance exhibited a decreasing trend. The numerical simulations were initiated with a model of the beam under no load, ensuring the beam was properly supported and the boundary conditions matched the experimental setup. A gradually increasing load was applied to the model to simulate the conditions experienced during the experimental tests. This load was incremented in small steps to capture the detailed load–deflection behavior and moment distribution along the beam. During the simulation, the moment at each increment was

calculated, and the process continued until the beam reached its ultimate load-carrying capacity, indicating failure. This ultimate moment was then recorded as the peak value in the moment distribution.

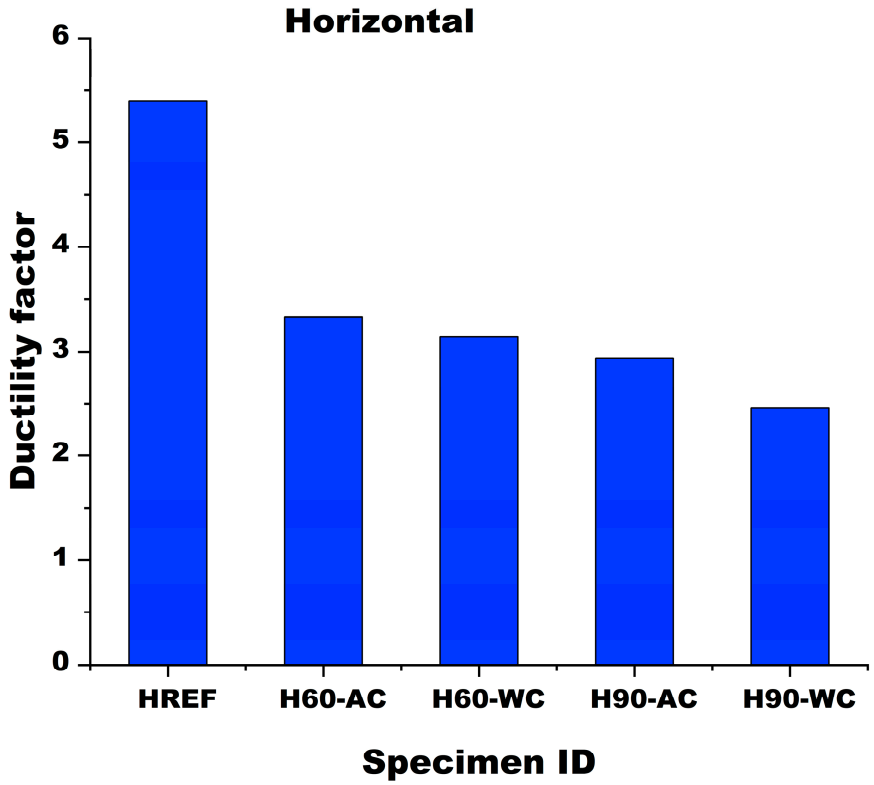

Figure 19. Ductility factor for sections with horizontal stiffener.

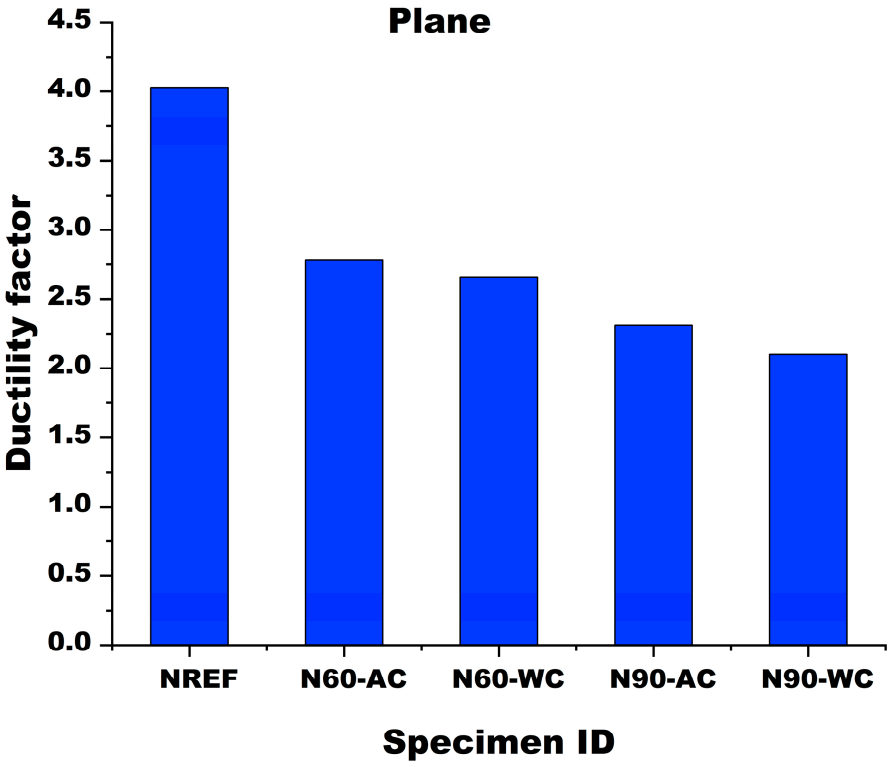

Figure 20. Ductility factor for sections with no stiffener.

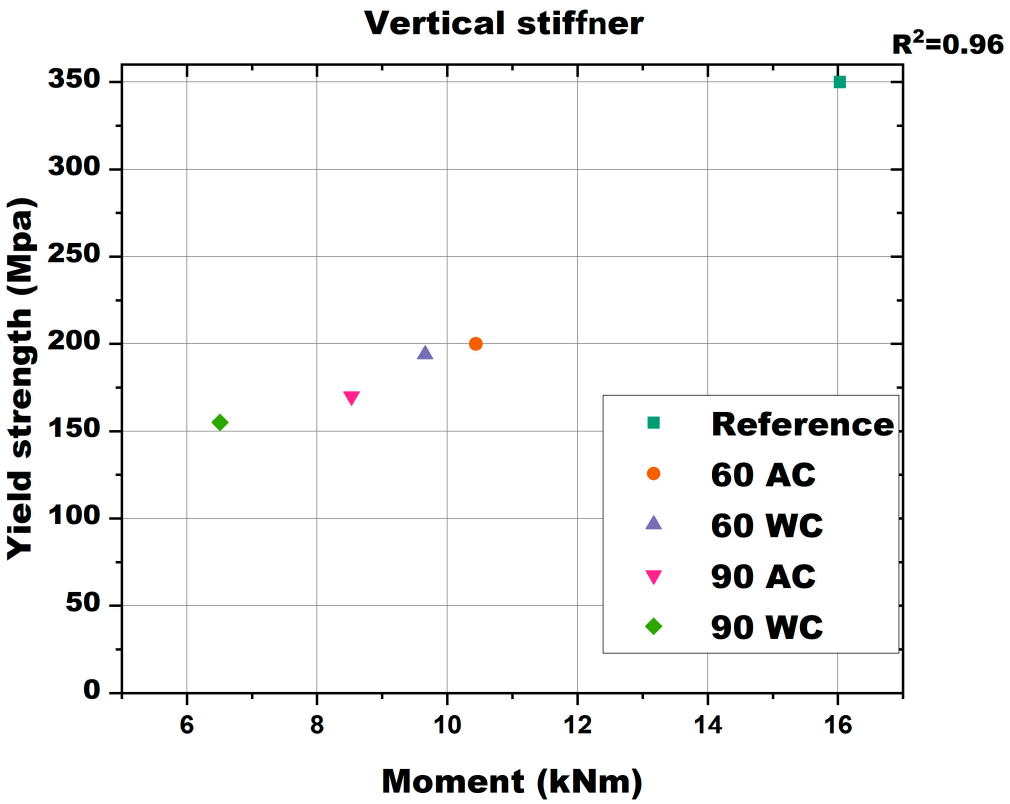

Figure 21. Relationship obtained between yield strength and the moment with vertical stiffener.

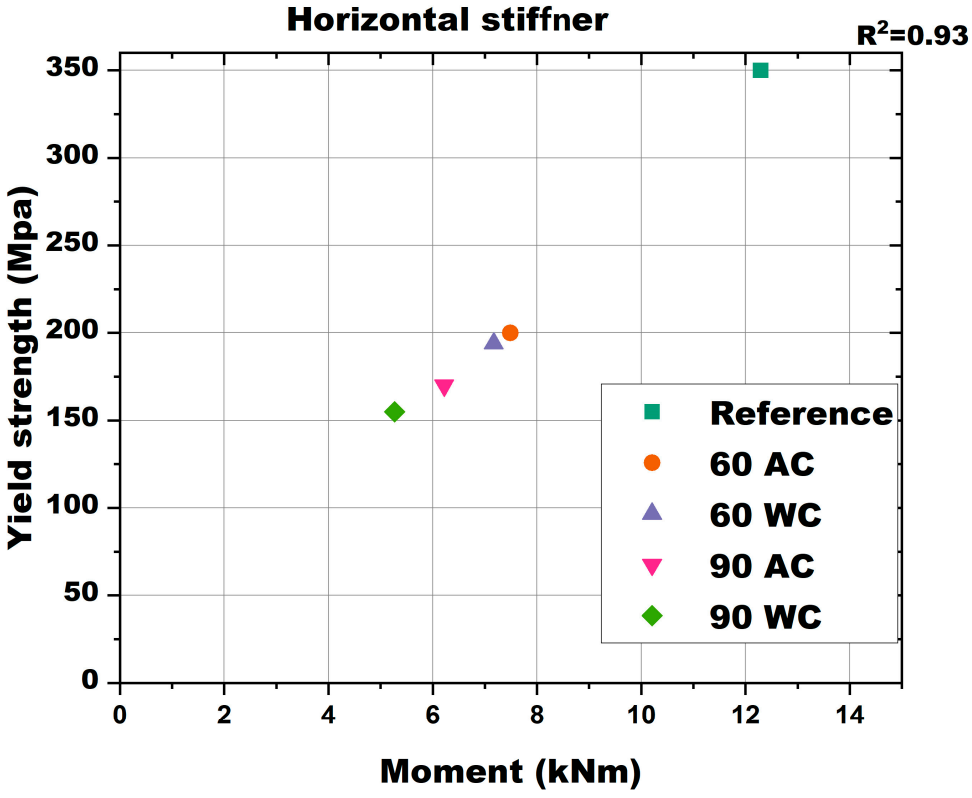

Figure 22. Relationship obtained between yield strength and the moment with horizontal stiffener.

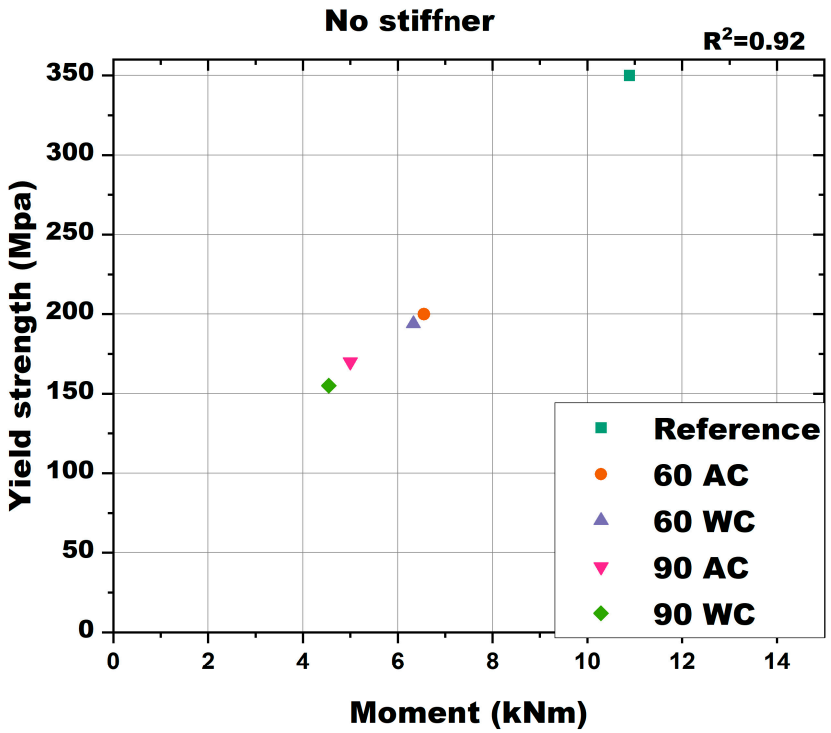

Figure 23. Relationship obtained between yield strength and the moment with no stiffener.

4. Direct Strength Method

The theoretical analysis of results considers the configuration of built-up members and their connections. Determining the effective area using the effective width method proves challenging due to the nature of built-up members and intermittent connections. Furthermore, current design codes lack specific guidelines for designing members post-fire, primarily due to difficulties in determining temperature distribution—whether uniform or non-uniform—across members. As an alternative approach, coupon test results are utilized for designing members after fire exposure.

The Direct Strength Method (DSM) provides a straightforward approach to understanding the buckling behavior of members. This method involves determining section properties and conducting elastic buckling analysis, typically using software like CUFSM [26]. Therefore, this section evaluates the conservativeness of DSM in predicting the behavior of structural members. The numerical results from ABAQUS and the analytical results from DSM were compared to these experimental findings to assess the accuracy of the models.

DSM is applied to establish the design moment capacities of structural members. Sectional properties critical for analysis are derived from coupon tests. Buckling analysis is performed using specialized software, such as CUFSM [26]. Equations (3)–(5) used in the DSM method are outlined below:

$$M_{nd} = M_y + \left(1 - \frac{1}{C^2_{yd}}\right)(M_p - M_y)\ for\ \delta_d \leq 0.673 \tag{3}$$

$$M_{nd} = \left[1 - 0.22\left\{\frac{M_{crd}}{M_y}\right\}^{.5}\right]\left\{\frac{M_{crd}}{M_y}\right\}^{.5} M_y\ for\ \delta_d \geq 0.673 \tag{4}$$

where

M_{nd}—Nominal moment capacity considering the distortional buckling limit state;
M_y—Member yield moment;
M_{crd}—Critical elastic distortional buckling moment;

C_{yd} -Distortional buckling coefficient that modifies the nominal flexural strength;

$$\delta_d - \sqrt{\frac{M_y}{M_{crd}}} \tag{5}$$

Table 4 presents the moments calculated for all sections using the DSM method and the loads obtained through FEM and experimental tests [27]. The mean and coefficient of variation are also calculated and displayed in the table. Figure 24 shows the signature curves of reference specimens obtained for CFS beams with vertical stiffener. The signature curve illustrates the relationship between flexural strength and slenderness of a structural member, which is crucial for understanding the buckling behavior of cold-formed steel members under various loading conditions, such as axial compression, bending, and shear [26,30]. This curve helps identify the critical buckling load, which is vital for evaluating stability. By plotting the load against slenderness, one can pinpoint the buckling threshold of the member. Typically, as slenderness increases, the member's strength decreases, a trend captured by the curve. This reduction in strength is visually and analytically represented, allowing for predictions on how the member will behave under increasing slenderness. Additionally, the curve aids in calibrating parameters for the Direct Strength Method (DSM) equations, ensuring that the DSM provides accurate and conservative strength predictions for cold-formed steel members.

Table 4. Comparison of load of all the specimens obtained through experimental, analytical, and DSM methods.

Sl No	Specimen IDs	Experimental Load (kN)	Experimental Moment (kNm)	FEM Load kN	FEM Moment (kNm)	DSM Moment (kNm)	M_{EXP}/M_{FEM}	M_{EXP}/M_{DSM}	M_{FEM}/M_{DSM}
1	EREF	64.30	15.72	71.26	16.12	15.66	0.98	1.00	1.03
2	E60-AC	48.40	12.95	50.21	13.24	14.31	0.98	0.90	0.93
3	E60-WC	36.53	9.42	40.29	10.52	14.03	0.90	0.67	0.75
4	E90-AC	29.10	7.43	37.95	7.94	11.32	0.94	0.66	0.70
5	E90-WC	26.20	6.21	28.94	6.82	10.73	0.91	0.58	0.64
			Mean				0.94	0.76	0.81
			COV				0.05	0.10	0.10

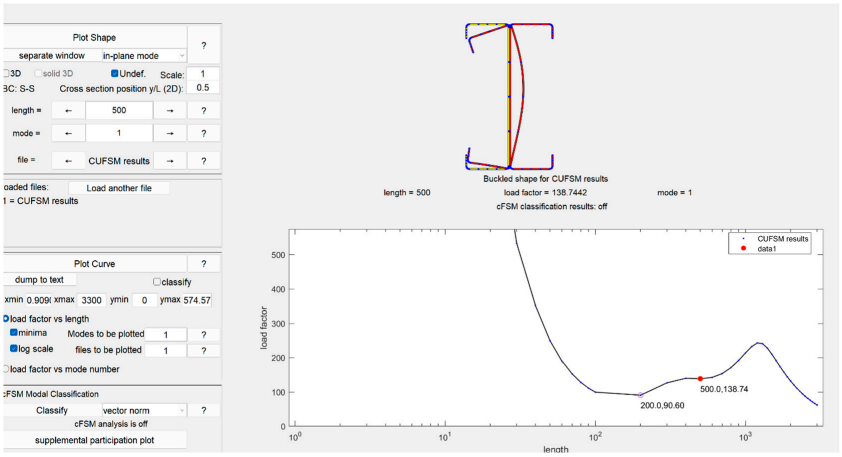

Figure 24. Signature curve for beam section EREF.

5. Conclusions and Scope for Future Studies

This study investigated the flexural behavior of GI-based CFS beam sections subjected to elevated temperatures and cooled using water and air under two-point loading. The

beams used were of grade G350. Experimental findings were validated through Finite Element Modeling (FEM), and parametric studies were conducted on beams with horizontal stiffeners and without stiffeners. Moment capacities were calculated using the Direct Strength Method (DSM) and compared across different beam configurations. While this study focuses on immediate structural performance, the insights gained can inform corrosion mitigation strategies in long-term applications.

Key conclusions drawn from this study are outlined below:

- Parametric analysis confirmed that different stiffener configurations did not alter the predominant failure mode, which remained distortional buckling across all specimens.
- Beams with vertical and horizontal stiffeners consistently exhibit distortional buckling during various heating and cooling durations. In contrast, unstiffened sections fail through both distortional and lateral–torsional buckling, with lateral–torsional buckling typically occurring first.
- Distortional buckling primarily occurred in the middle section of the beams, with local buckling observed at stiffeners and web lips.
- The provision of restrained supports and additional stiffeners at loading points effectively prevented lateral–torsional buckling.
- Beams with vertical stiffeners demonstrated superior performance compared to those with horizontal stiffeners in parametric analysis.
- Lateral–torsional buckling was observed in the reference specimen lacking stiffeners due to inadequate restraint at the supports.
- During validation, the comparison between experimental results and FEM analysis demonstrated strong agreement, and failure modes obtained from both analyses matched, indicating that the modeled simulations accurately represent the physical behavior of the structures. This consistency underscores the reliability and precision of the FEM models in capturing key aspects of the structural performance.

Scope for Future Studies:

- Future studies could explore the behavior of stainless steel-, mild steel-, and aluminum-based industrial purlin sections under similar conditions.
- Investigate the effects of higher thermal exposures on unsymmetrical sections to understand their performance and structural integrity.

Author Contributions: Methodology, V.S.S. and A.N.; Validation, G.W.K.M. and K.R.; Formal analysis, V.S.S., G.W.K.M. and K.R.; Investigation, V.S.S.; Resources, G.W.K.M.; Data curation, V.S.S., G.W.K.M. and B.G.A.G.; Writing—original draft, A.N., D.A., B.G.A.G. and K.R.; Writing—review & editing, A.N. and K.R.; Visualization, D.A. and B.G.A.G.; Supervision, A.N. and D.A.; Project administration, A.N. and D.A. All authors have read and agreed to the published version of the manuscript.

Funding: This research received no external funding.

Institutional Review Board Statement: Not applicable.

Informed Consent Statement: Not applicable.

Data Availability Statement: No new data were created or analyzed in this study. Data sharing is not applicable to this article.

Conflicts of Interest: The authors declare no conflict of interest.

References

1. *AISI S100-07/S2-10*; North American Specification for the Design of Cold-Formed Steel Structural Members, Supplement No. 2. American Iron and Steel Institute: Washington, DC, USA, 2010.
2. Code, P. Eurocode 3: Design of steel structures—Part 1–2: General rules—Structural fire design. *J. Constr. Steel Res.* **2005**, *54*, 9–56.
3. Wan, H.X.; Huang, B.; Mahendran, M. Experiments and numerical modelling of cold-formed steel beams under bending and torsion. *Thin-Walled Struct.* **2021**, *161*, 107424. [CrossRef]
4. Yun, X.; Meng, X.; Gardner, L. Design of cold-formed steel SHS and RHS beam–columns considering the influence of steel grade. *Thin-Walled Struct.* **2022**, *171*, 108600. [CrossRef]

5. Shakarami, M.; Zeynalian, M.; Ataei, A. Numerical study of the behavior of friction-grip bolted shear connectors in composite beams with cold-formed steel sections. *Thin-Walled Struct.* **2023**, *184*, 110539. [CrossRef]
6. Chen, Z.; Huang, Y.; Young, B. Design of cold-formed ferritic stainless steel RHS perforated beams. *Eng. Struct.* **2022**, *250*, 113372. [CrossRef]
7. Karthik, C.; Anbarasu, M. Cold-formed ferritic stainless steel closed built-up beams: Flexural behaviour and numerical parametric study. *Thin-Walled Struct.* **2021**, *164*, 107816. [CrossRef]
8. Ungureanu, V.; Both, I.; Burca, M.; Radu, B.; Neagu, C.; Dubina, D. Experimental and numerical investigations on built-up cold-formed steel beams using resistance spot welding. *Thin-Walled Struct.* **2021**, *161*, 107456. [CrossRef]
9. Pawanithiboworn, K.; Pannachet, T.; Boonpichetvong, M. Investigation of Parameters Affecting Rotational Behavior of Cold-Formed Steel Connection. *Civ. Eng. J.* **2023**, *9*, 2752–2769. [CrossRef]
10. Li, Q.Y.; Young, B. Experimental and numerical investigation on cold-formed steel built-up section pin-ended columns. *Thin-Walled Struct.* **2022**, *170*, 108444. [CrossRef]
11. Jaya Kumar, G.; Kiran, T.; Anand, N.; Anbarasu, M.; Lubloy, E. Post-fire flexural behaviour and performance of unrestrained cold-formed steel built-up section beams: Experimental and numerical investigation. *Case Stud. Constr. Mater.* **2023**, *18*, e01978. [CrossRef]
12. Jaya Kumar, G.; Kiran, T.; Anand, N.; Al-Jabri, K. Influence of fire-resistant coating on the physical characteristics and residual mechanical properties of E350 steel section exposed to elevated temperature. *J. Struct. Fire Eng.* **2023**, *14*, 228–253. [CrossRef]
13. Hareindirasarma, S.; Elilarasi, K.; Janarthanan, B. Effect of circular holes on the web crippling capacity of cold-formed LiteSteel beams under Interior-Two-Flange load case. *Thin-Walled Struct.* **2021**, *166*, 108135. [CrossRef]
14. Gjukaj, A.; Salihu, F.; Muriqi, A.; Cvetanovski, P. Numerical Behavior of Extended End-Plate Bolted Connection under Monotonic Loading. *HighTech Innov. J.* **2023**, *4*, 294–308. [CrossRef]
15. Laím, L.; Rodrigues, J.P.C.; da Silva, L.S. Experimental and numerical analysis on the structural behaviour of cold-formed steel beams. *Thin-Walled Struct.* **2013**, *72*, 1–13. [CrossRef]
16. Both, I.; Burca, M.; Benzar, S.; Ungureanu, V. Numerical Study on the Behaviour of Built-up Cold-Formed Steel Corrugated Web Beams End Connections. *Civ. Eng. J.* **2023**, *9*, 770–786. [CrossRef]
17. Kankanamge, N.D.; Mahendran, M. Behaviour and design of cold-formed steel beams subject to lateral–torsional buckling at elevated temperatures. *Thin-Walled Struct.* **2012**, *61*, 213–228. [CrossRef]
18. "EN 1993-1-1". 2005. Available online: https://www.phd.eng.br/wp-content/uploads/2015/12/en.1993.1.1.2005.pdf (accessed on 4 February 2024).
19. Wang, L.; Young, B. Behaviour and design of cold-formed steel built-up section beams with different screw arrangements. *Thin-Walled Struct.* **2018**, *131*, 16–32. [CrossRef]
20. Wang, H.; Zhang, Y. Experimental and numerical investigation on cold-formed steel C-section flexural members. *J. Constr. Steel Res.* **2009**, *65*, 1225–1235. [CrossRef]
21. Landesmann, A.; Camotim, D. Distortional failure and DSM design of cold-formed steel lipped channel beams under elevated temperatures. *Thin-Walled Struct.* **2016**, *98*, 75–93. [CrossRef]
22. Rodrigues, J.P.C.; Laim, L.; Craveiro, H.D. Influence of web stiffeners on cold-formed steel beams subjected to fire. *J. Struct. Fire Eng.* **2016**, *7*, 249–261. [CrossRef]
23. Roy, K.; Lim, J.B.; Lau, H.H.; Yong, P.M.; Clifton, G.C.; Johnston, R.P.; Wrzesien, A.; Mei, C.C. Collapse behaviour of a fire engineering designed single-storey cold- formed steel building in severe fires. *Thin-Walled Struct.* **2019**, *142*, 340–357. [CrossRef]
24. Pannuzzo, P.; Chan, T.-M. Flexural behaviour of cold-formed steel square and rectangular hollow sections with moderate heat-treatment. *J. Constr. Steel Res.* **2022**, *197*, 107454. [CrossRef]
25. Zhu, J.-H.; Su, M.-N.; Zhu, X.; Daniels, J.; Young, B. Flexural behaviour of cold-formed steel oval hollow section beams. *J. Constr. Steel Res.* **2021**, *180*, 106605. [CrossRef]
26. *CUFSM*, Version 5.01; John Hopkins University: Baltimore, MD, USA, 2018.
27. Sam, V.S.; Nammalvar, A.; Andrushia, D.; Gurupatham, B.G.A.; Roy, K. Flexural Behavior of Galvanized Iron Based Cold-Formed Steel Back-to-Back Built-Up Beams at Elevated Temperatures. *Buildings* **2024**, *14*, 2456. [CrossRef]
28. *Abaqus Analysis User's Manual (2018)*; ABAQUS Analysis User's Manual-Version 6.14-2; ABAQUS: Flower Mound, TX, USA, 2018.
29. Sam, V.S.; Anand, N.; Marak, G.W.K.; Lyngdoh, G.R.; Alengaram, J.; Andrushia, D. Investigation on Residual Mechanical Properties of Galvanized Iron Cold-Formed Steel Sections Exposed to Elevated Temperatures. *Electron. J. Struct. Eng.* **2024**, *24*, 53–59. [CrossRef]
30. Chen, J.; Young, B. Experimental investigation of cold-formed steel material at elevated temperatures. *Thin-Walled Struct.* **2007**, *45*, 96–110. [CrossRef]